FFI-rapport 2014/00260

Low-frequency long-range atmospheric noise propagation modelling with the PE method

Knut Waagan

FFI Forsvarets forskningsinstitutt

FFI-rapport 2014/00260

Low-frequency long-range atmospheric noise propagation modelling with the PE method

Knut Waagan

Norwegian Defence Research Establishment (FFI)

6 February 2014

FFI-rapport 2014/00260

382001

P: ISBN 978-82-464-2346-3
E: ISBN 978-82-464-2347-0

Keywords

Støy

Akustikk

Beregning

Lavfrekvent

Skytefelt

Approved by

Eirik Svinsås	Project Manager
Stein Grinaker, Svein Rollvik	Director of Research
Jon Skjervold	Director

English summary

This note is part of an effort to improve numerical prediction of acoustic noise from Norwegian military practice ranges. The focus is on low-frequency, long-ranging sound. A Parabolic Equation method for sound propagation is summarised, implemented and tested. This method is considered because of its ability to take into account quite general terrain data and sound speed profiles. The implementation is validated against examples from the research literature. Numerical parameter choices for low frequencies that ensure adequate accuracy are determined, and the resulting computational efficiency is assessed. Some studies of physical parameter variation are included. They demonstrate the code's abilities, and provide some basic insights on model sensitivity.

Sammendrag

Dette notatet er er del av et arbeid for forbedre numerisk prediksjon av akustisk støy fra norske skyte- og øvingsfelt. Vi fokuserer på lavfrekvent og vidtrekkende lyd. En 'Parabolic Equation'-metode for lydutbredelse blir oppsummert, implementert og testet. Grunnen til at vi ser på denne metoden er at den kan ta i bruk nokså generelle terrengdata og lydhastighetsprofiler. Implementasjonen blir validert mot eksempler fra forskningslitteraturen. Numeriske parametervalg som gir adekvat nøyaktighet blir bestemt, og den resulterende regneeffektiviteten måles. Noen studier med variasjon i fysisk parametre er inkludert. Studiene demonstrerer mulighetene koden har, og gir noen grunnleggende innsikter.

Contents

1 Introduction

This note concerns numerical prediction of sound propagation through the near-ground atmosphere. The specific application in mind is blast noise from the Norwegian Defence's shooting ranges, where noise annoyance of neighbouring civilians must be kept low and under control. Forsvarsbygg uses the software Milstøy II, developed at Sintef, to produce noise maps. A new version called Milnoise is underway. Various computational algorithms are included in this code, some based on measurements, some based on simplified acoustic models. In this note, we consider a prospective theory-based algorithm, termed the Parabolic Equation (PE) Method, which can handle realistic weather and ground data.

Characteristic features of military noise are low frequency content (down to a few Hz), long range (up to 10-20 km), short duration and nonlinear propagation near the source. The majority of research work on environmental noise is driven by traffic and industrial noise, which is comparatively high frequent, short-ranging, of longer duration and propagates linearly. Most methodology in Milnoise is taken from traffic noise models, which leaves a need for better handling of low frequencies and long ranges. These two requirements largely coincide for two reasons: The loudest noise sources are low frequent, and high frequency signals are dissipated significantly in the air. The handling of nonlinearity is in typical practice incorporated in source modelling and will not be discussed here (some references are [5, 14]). Temporal aspects are not directly discussed as computations are performed in the frequency domain.

We base our methodology around [8]. A second good general reference for outdoor noise propagation is [1]. Some more mathematical detail about the PE method can be found in [6]. A good summary of more recent developments long-range outdoor acoustics can be found in [16].

The purpose of this note is to document the code we are developing and to justify choices of parameters and strategies therein. The main focus is on numerical issues, but critical modelling issues are also summarised and illustrated with examples. Both computational accuracy and efficiency are discussed.

2 Summary of the Parabolic Equation Method

Since we largely follow the text book [8], we only provide a brief summary of the parabolic equation model here. The main PDEs and boundary conditions will be explicitly and succinctly stated in the following. In the model, radial symmetry is assumed, hence only two coordinates, the range r (horizontal distance from source) and the vertical axis z are used. This means we have to solve the Helmholtz equation for each frequency f, given by

$$q_{rr} + q_{zz} + k^2 q = 0, \quad k = 2\pi f/c, \quad q(r,z) = \sqrt{r} p_c(r,z). \tag{2.1}$$

We write the temporal Fourier transform of the pressure as p_c. The sound speed c can vary spatially. At the ground we obtain closure with an impedance boundary condition

$$p_z = -\frac{ik_a}{Z}p. \tag{2.2}$$

The normalised impedance value Z depends on the frequency and ground properties.

Derivation of the Parabolic equation approximation is based on restricting attention to sound waves propagating away from source and not too steeply. The simplest form is the narrow angle equation

$$2ik_a\Psi_r + \Psi_{zz} + (k^2 - k_a^2)\Psi = 0, \quad p_c(r,z) = \Psi(r,z)e^{ik_a r}/\sqrt{r}. \tag{2.3}$$

Here k_a is a typical wave number (we use the k-value at the ground). Note that (2.3) is basically a Schrödinger equation with r taking the place of time. Hence it is a well known parabolic PDE. This brings us to the main point: The approximation (2.3) is much quicker to solve numerically than the elliptic Helmholtz equation. Or strictly speaking, once we know Ψ as a function of z at the source position $r = 0$, it is quicker to solve. Salomons suggests an analytical approach to set the starting data $\Psi(0,z)$ which we follow here (the forms (G.75) and (G.78) in [8] are used unless stated otherwise).

The narrow angle equation has, for $k = k_a$ (iëin the absence of refraction), Fourier solutions

$$\Psi(r,z) = \Psi_0 \exp[i(lz - l^2 r/2k_a)], \tag{2.4}$$

where l is an arbitrary wave number in the z-direction. This is, in light of the Schrødinger equation analogy, recognisable as a plane wave with phase speed $l/2k_a$. The phase speed is a Taylor-expansion around $l = 0$ to the exact phase speed $(1 - \sqrt{1 - (l/k_a)^2})k_a/l$ resulting from the Helmholtz equation (the physical meaning of this 'phase speed' is a propagation direction). Conservation of energy is implied in the form

$$\left(\frac{1}{2}|\Psi|^2\right)_r - \frac{1}{2k_a}\left(\ \mathrm{Re}(\Psi)\mathrm{Im}(\Psi_z) - \mathrm{Re}(\Psi_z)\mathrm{Im}(\Psi)\ \right)_z = 0. \tag{2.5}$$

At the impedance boundary the energy flux is $-\mathrm{Re}(1/Z)\frac{1}{2}|\Psi|^2$.

For outdoor sound propagation the following more accurate 'wide angle' approximation is most often used

$$\left(1 + \frac{1}{4k_a^2}L_1\right)\Psi_r - \frac{i}{2k_a}L_1\Psi = 0, \quad L_1 = \frac{\partial^2}{\partial z^2} + (k^2 - k_a^2). \tag{2.6}$$

The phase speed is adjusted to

$$[1 - (l/2k_a)^2]^{-1}\frac{l}{2k_a},$$

a Padé approximation of the exact case. Note the blow-up at the (unphysical) wave number $l = 2k_a$. A much less used, but about equally accurate parabolic model, is

$$2ik_a\Psi_r + \Psi_{zz} + \frac{i}{4k_a^2}\Psi_{zzzz} + (k^2 - k_a^2)\Psi = 0. \tag{2.7}$$

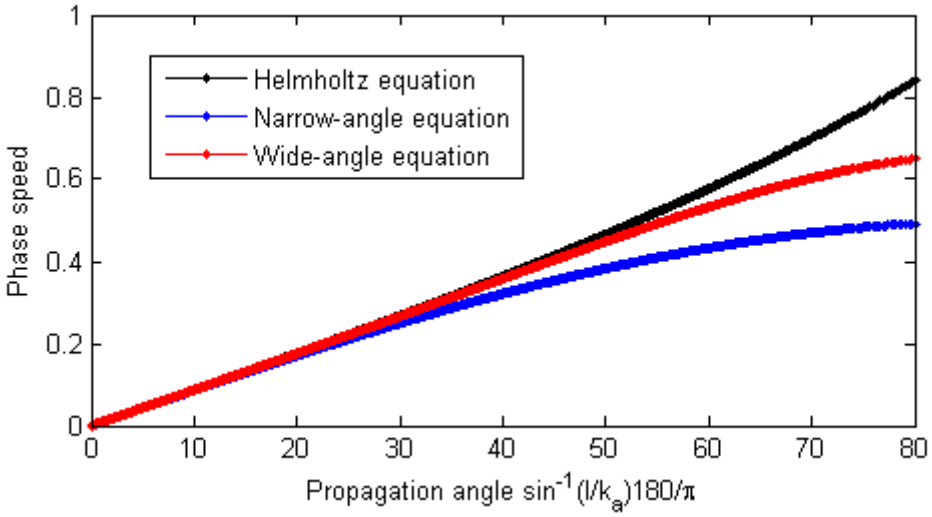

Figure 2.1 The 'phase speed in the models. The x-axis shows the propagation angle of the wave in the exact case. The wide-angle form shown is the Padė approximation

Its phase speed is simply $l/2k_a + l^3/8k_a^3$, a higher order Taylor expansion of the exact case. The reason (2.6) is preferred over (2.7) is that (2.7) requires larger numerical stencils, leading to lower computational efficiency and complicated boundary treatment. The respective phase speeds in the models are plotted as a function of propagation angle in Figure 2.1. The wide angle model is indistinguishable from the exact up to 35°. This gives a simple visual justification of the parabolic approximation. More sophisticated derivations can be found in the literature.

2.1 Terrain

The above procedure works for flat topography. In order to treat more general topography, we approximate it with a piecewise linear terrain profile. For each linear range section with altitude $H(r) = H_0 + Cr$, we use the following generalisation of the wide angle PE (2.6):

$$\Psi_r + \frac{i}{2k_a} L_1\Psi + \frac{1}{4k_a^2} L_1\Psi_r + \frac{i}{k_a} C\Psi_{zr} = 0. \tag{2.8}$$

In this model z denotes height above ground. Equation (2.8) is a special case of the GTPE for general smooth terrain included in [8]. The differential operator L_1 is defined by

$$L_1\Psi = (C^2+1)\Psi_{zz} - 2ik_aC\Psi_z + (k^2 - k_a^2)\Psi. \tag{2.9}$$

Nonrefractive Fourier solutions have the form

$$\Psi_l(r,z) = \exp\left(ilz + i\frac{A}{2k_a}\left(1 + \frac{A}{4k_a^2} - \frac{l}{k_a}C\right)^{-1}\right), \quad A = -(C^2+1)l^2 + 2k_aCli. \tag{2.10}$$

Note that $l = 0$ corresponds to a wave that propagates parallel to the ground. The impedance boundary condition at the ground becomes

$$\Psi_r \sin\alpha - \Psi_z(\cos\alpha)^{-1} = \frac{ik_a}{Z}\Psi - ik_a\Psi\sin\alpha, \quad \alpha = \tan^{-1} C. \tag{2.11}$$

2.2 Physical effects and data

Data input to the propagation model consists of the the specific ground impedance Z and the effectice sound speed c. There are big uncertainties in both quantities. For the weather conditions the main challenges are fluctuations and difficulty of measurement. Research in outdoor acoustics often essentially consists of describing the environment, i. e. sound speed variation and ground properties, and describing the sensitivity of sound levels to environmental parameters. General references are the textbooks [8] and [1]. For more recent developments, a good review is given in [16]. In this report we only briefly summarise the models we have implemented and tested.

For the ground interaction, basic modelling is difficult. We calculate the impedance Z from the rigid frame porous model of [12], as was suggested in [11]. This impedance model requires as its single input quantity the ground resistivity. We also use a generalisation of this one-parameter model to a rigid frame porous layer over a hard (fully reflecting) surface. We remark that this impedance boundary for a hard backed layer is derived by the taking the grazing angle limit value of Z, which is reasonable for our application (see e. g. [4, 13]).

The effective sound speed is defined as the sound speed plus the wind component in the horizontal propagation direction, which constitutes a widely used approximation. For now, we assume that the sound speed only varies with the height z above ground. A realistic form (at least in homogeneous terrain) that we will use as an example, is the loglin model [2]:

$$c(z) = c_0 + c_1 z/z_l + c_2 \log(z/z_0 + 1), \quad z_l = 1\text{m}. \tag{2.12}$$

The parameter z_0 is called the roughness length, and is regarded as a property of the terrain. A typical value for grassland is 0.1 m. For woodland $1 - 10$ m is reasonable. The gradient $c'(z)$ is of greatest interest. When $c'(z) < 0$ there is upward refraction and there will be a 'shadow' zone near the ground. When $c'(z) > 0$ there is 'downward refraction' and sound energy is directed towards the the ground, resulting in increased sound levels. Downward refraction typically occurs during temperature inversions, and for downwind propagation.

We have incorporated turbulent fluctuations according to the model in [8]. It is a stochastic model, consisting of an algorithm for constructing realisations of the perturbation μ to the mean refractive index c_0/c. The correlation function $\mathrm{E}[\mu(r + \delta r, z + \delta z)\mu(r, z)]$ behaves according to a desired turbulence model with Gaussian and Von Karman correlation function given. The von Karman correlation model is reported to give good results and is used here. Only isotropic models are considered with horizontal and vertical correlations equal. It is a computationally expensive model since Monte Carlo sampling is needed to obtain statistics, and also because generating a realisation is costly.

In practice turbulent fluctuations have two important effects: One is that narrow interference minima are obscured, making them difficult to predict with deterministic methods. The second is that acoustic energy is scattered into shadow regions. therefore the non-turbulent simulations tend to underestimate noise in shadow regions.

2.3 Implementation

We use the finite difference scheme from [8] to solve the parabolic equation. The grid is uniform, and z-derivatives are replaced with standard second order discrete forms. The Crank-Nicolson method is used to advance the solution in the range direction, analogously with its typical usage for time integration. Crank-Nicolson has the advantage of being unconditionally stable as well as non-dissipative. For long-range sound propagation it is important to avoid numerical dissipation, as it will lead to underestimation of sound levels. The lack of dissipation can sometimes be a weakness, as it may lead to spurious oscillations when there are insufficiently resolved features. Such issues are discussed in [6].

We have implemented the numerical algorithm in Matlab. Care has been taken to ensure efficiency by using the right built-in Matlab features. The most time-consuming part is the solution of a tridiagonal linear system at each range step. The Matlab sparse grid type was hence found crucial for efficiency. The tridiagonal matrix M of the associated system changes each time the ground slope C changes. Rebuilding M and solving the new system is costly, while in contrast, when C stays constant we can apply sparse LU-decomposition to M and use the result until C changes again. The code is able to take advantage of this, by dividing the range into sections of constant slope. One small numerical detail should be noted about the range sections: The discrete version of the terrain boundary condition (2.11) approximates Ψ_r with a second-order one-sided derivative $(-2\Psi^n + 1.5\Psi^{n-1} - 0.5\Psi^{n-2})/\Delta r$. For the first range step, the furthest data point Ψ^{n-2} is missing. A first-order one-sided derivative $(\Psi^n - \Psi^{n-1})/\Delta r$ can be used instead, as is standard procedure for multi-step schemes. In our case, each time we start on a new range section (usually because the slope C changes), we have to resort to the first order boundary discretisation. Technically, this reduces the order of accuracy of the scheme when range sections are small. In practice the effect is miniscule, as can be verified for a case with constant slope throughout the range.

The code can handle height varying sound speed, and range variation in impedance. Range-varying sound speed profiles only requires a simple extension. In order to make it easy to change the parameters, there are separate functions for the data inputs. The stochastic atmospheric turbulence model described in [8] has been implemented to generate turbulent fluctuation in the sound speed.

3 Computational examples from the literature

We first consider some examples taken from the literature. They serve to validate our implementation, and to illustrative some important physical effects. The output quantity of interest is the relative sound level ΔL measured in dB. It is defined by

$$\Delta L = 10\log_{10}\frac{\|p\|^2}{\|p_{\text{free}}\|^2}, \quad p_{\text{free}} = S\frac{e^{ik\sqrt{r^2+z^2}}}{\sqrt{r^2+z^2}}, \tag{3.1}$$

where p_{free} is the complex sound pressure due to a free sound source (i.e. absent of refraction and ground interaction). Consequently, the measured sound level L_p in dB equals the sum of the free

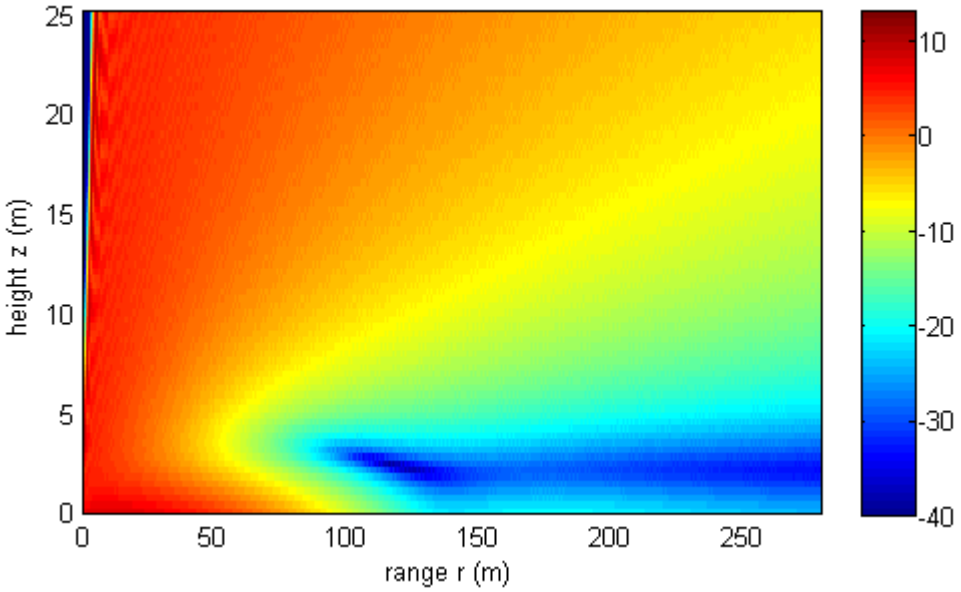

Figure 3.1 Relative sound levels for $100Hz$ *over snow computed with the PE code.*

source sound level in dB plus ΔL, regardless of source strength S. The sound speed is set to 340 m/s near the ground in all examples.

3.1 Ground effect example

An interesting example is given in the report [4]. It demonstrates a ground effect which the standard methods in Milstøy do not model. The impedance boundary condition corresponds to a 14.5 cm thick layer of soft snow over a hard surface. Figure 3.1 shows relative sound levels from our PE calculation. We observe good agreement with the figure from [4], which was produced with an analytical, but computationally inefficient, formula. The PE calculation took about 0.3 s on a laptop. Evidently, the PE method can handle surface wave phenomena provided the ground can be represented by an impedance boundary. One feature to notice is the large variation with height below 5m. There is a 'quiet height' that persists from about $r = 100$m.

3.2 Examples by Salomons

Salomons [8] includes illustrative examples of PE computations. They can be used for validating our implementation. We show here only a few of the more complicated cases from the book. Figure 6.4 from [8] demonstrates upwind propagation over a hill at $f = 300$ Hz. The shape of the hill is only provided graphically, so we approximate it using a cosine-shape peaking at a height of $10m$ at $r = 175$m and with period of 250 m. Our resulting sound level graph, Figure 3.2, still agrees well with [8]. A flat ground simulation is included in the plot for comparison. Note that the hill feature has an effect of roughly 5dB even several hundred meters into the flat zone. On and just behind the hill itself the effect is large.

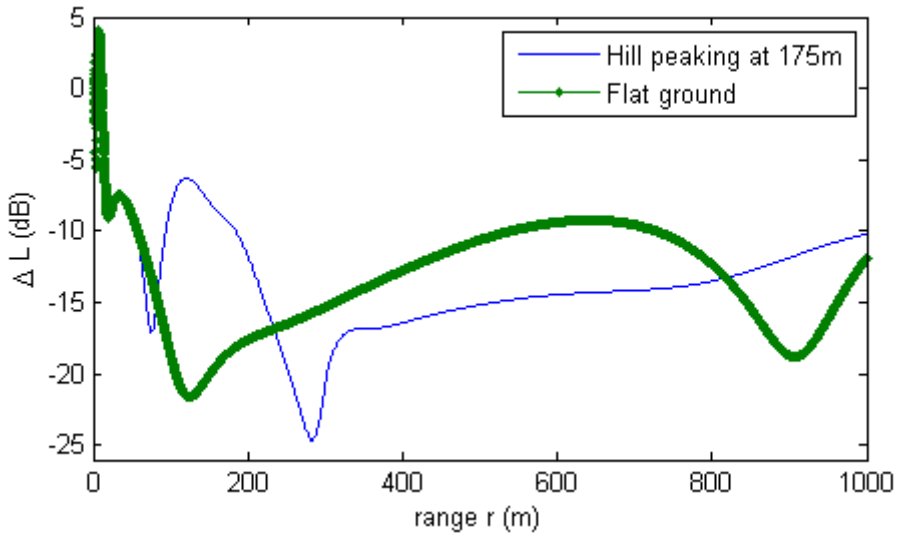

Figure 3.2 Relative sound level for 300 Hz source over terrain. Reproduction of Figure 6.4 in Salomons' book. Source and receiver were both at 2 m above ground, and ground properties given by $\sigma = 200$*kPa s/m*^{2}*. Sound speed of log-lin form* (2.12) *with* $c_1 = 0, c_2 = 1$ *m/s and* $z_0 = 0.1$ *m. These data could represent grassland vegetation.*

.

Another example considers $f = 500$ Hz and a hill we approximated by the same cosine-shape, this once peaking at ten meters height at $r = 375$ m and with period 500 m. Figure 3.3 shows the resulting sound levels above the topography. We obtain good qualitative agreement. Absent any refraction there is a strong shadow effect, while in the downward refraction case, interference patterns are the most prominent features. The turbulent simulation reveals intermittent scattering of sound energy into the shadow zone. In order to meaningfully describe the scattering pattern, computationally expensive random sampling is necessary, at least with presently known techniques. In many numerical experiments with turbulent shadow regions, the mean relative sound level ΔL reaches a range-independent minimum, however there exists no simple formula for such a minimum value. We also include a simulation with both downward refraction and the turbulence. The diffraction patterns are altered by the turbulence. We used the same turbulence parameters as in nonrefractive case. The largest mode in the realization of sound speed was of length 20π meters. We expect this is adequate to capture inertial range fluctuation effects, since modes near the sound wavelength dominate scattering. An artificial periodicity of about 20π meters is evident in this individual realization, though.

Note the quiet band that runs along the ground, most clearly in the downward refraction case. The turbulence simulation in Figure 3.3 indicates that the 'quiet height' also exists under atmospheric turbulence. Although sound levels fluctuate they stay low. The 'quiet height' effect has been studied in [15]. They concluded that it is a measurable and robust effect for night time downward refraction conditions in the range 100-500 Hz.

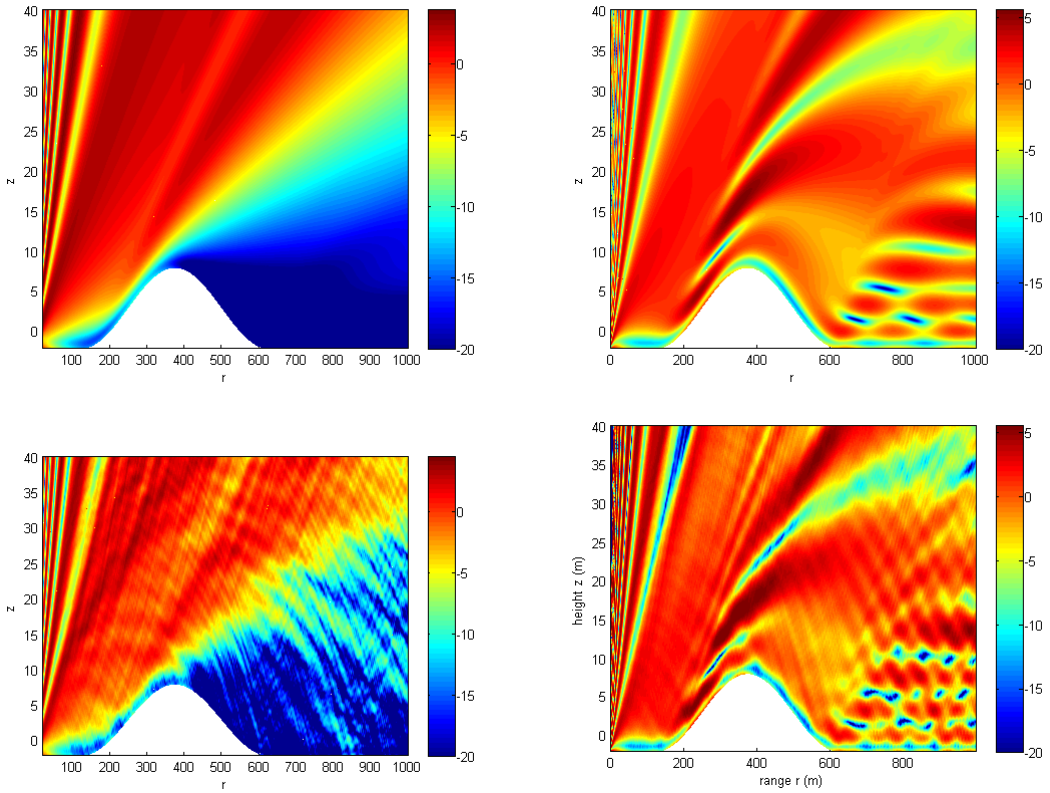

Figure 3.3 *Relative sound level (dB) for 500 Hz source over terrain. Reproduction of Figure 6.5 in Salomons' book. Source at 2 m above ground, and ground properties given by* $\sigma = 200$ *kPa s/m*^{2}*. UL: Constant atmosphere. UR: Downward refracting, sound speed of log-lin form* (2.12) *with* $c_1 = 0, c_2 = 1$ *m/s and* $z_0 = 0.1$ *m. BL: Constant atmosphere with turbulent fluctuations (Single realization). BR: Downward refracting atmosphere with turbulent fluctuations (Single realization). Note that zero height on the* y*-axis is set to the source height at 2 m above ground.*

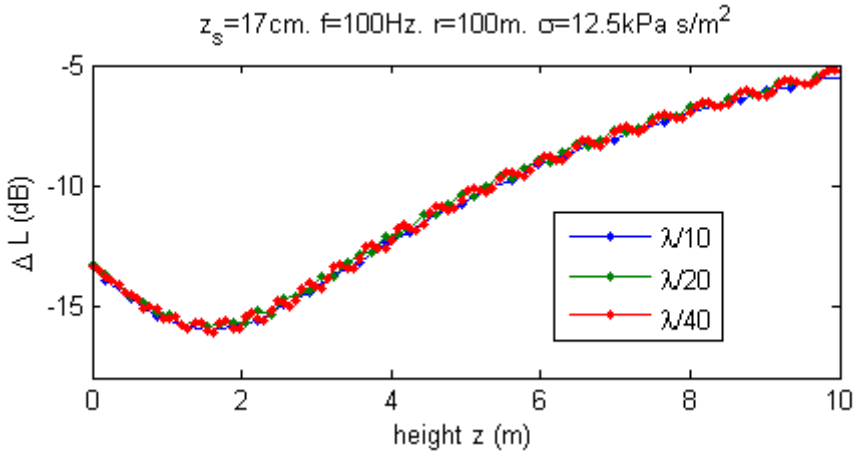

Figure 4.1 *Varying resolution with source height half a wavelength. We show vertical profiles of relative sound pressure at range* $r = 100m$.

4 Parameter studies

Most of the literature on PE methods does not address the low frequencies occuring in military applications. Therefore it is necessary to justify choices of numerical parameters with additional test simulations. In particular, Salomons recommends a grid resolution of one tenth wavelength both horizontally and vertically. This may lead to data features being insufficiently resolved when the wavelength is large. Once numerical parameters are set, it is also instructive to look at the effects of varying the physical parameters.

4.1 Resolution of source height

The source height may in some cases not be resolved by the grid resolution. This seems not to be an issue. For Figure 3.1, the source height was 1 cm above ground while the grid size was 34 cm. Figure 4.1 shows a case where the source is half a wave length above ground. Very soft soil is considered. At high resolution we see some oscillation. This feature persists under further refinement but has no practical significance. We conclude that source height should not influence numerical resolution. Instead, proper representation of a ground-near source is taken care of by the startdata alone.

4.2 Starting data

Salomons [8] uses a complicated analytical reprentation of a point source. Several versions of varied level of detail are suggested, and special care is taken to represent ground reflections when the source is near ground. The most and least sophisticated methods are compared in Figure 4.2 here. Analytical solution based on the grazing angle approximation is also shown. There are errors with all startdata types, but we get tolerable results provided the spherical reflection coefficient is used. Numerical resolution error was found to be dominated by the startdata error here by refinement tests. Possibly, more accuracy can be achieved with the method of [10]. Large errors

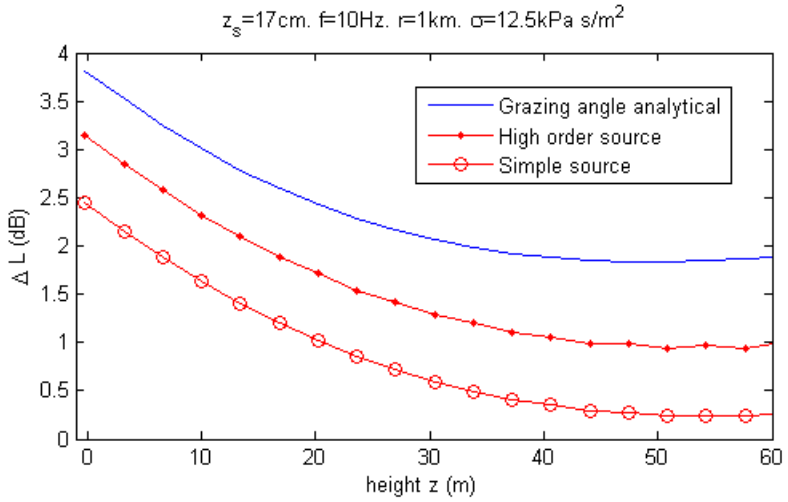

Figure 4.2 Startdata for near ground source. We show vertical profiles of relative sound pressure at range $r = 1$ km.

due to startdata was reported in that paper for hard ground, however our codes do not reproduce these. We conclude that the starting data (G.75) and (G.79) in [8] are adequate and efficient. For the exponential integral function in (G.79) we use the implementation included in Matlab.

4.3 Absorption layer and domain truncation

The absoption layer is clearly necessary for controlling reflections from the artificial upper boundary. Salomons does not provide absorption rates A_t for frequencies below 30 Hz. After some trial and error we found that a value $A_t = 0$ at $f = 0$ Hz with linear interpolation up to the 30 Hz value kept reflections under control. The layer thickness was kept to 50λ as recommended. With the absorption rate fixed, we tried to vary the thickness. For this experiment we considered a fully reflecting ground ($Z = \infty$), a range of 20 km, a frequency of 1 Hz, and log-shaped sound speed profiles with strengths $c_2 = -3, 0$ and 3 m/s respectively. The regular domain was 1 km high, a reasonable choice since sound rays reach a height of about 750 m ($\approx (2\pi c_0/c_2)^{-1/2} r$). The source height was 2 m. Resulting sound levels are plotted in Figure 4.3. We get acceptable errors at only 25λ, however we stick to the standard thickness for now. Even at 25λ, the absorption layer dominates computation time for the lowest frequencies. Errors are especially pronounced in the case of upward refraction, while the other weather scenarios are less sensitive to the layer thickness.

A second parameter of importance is the truncation height z_{top} of the regular domain. Using the same experimental setup as above we found some sensitivity to z_{top} in the upward refracting case , as seen in Figure 4.4. In practice, scattering by turbulence will probably have an impact, so this sensitivity is not very important. Taking the same height as we would for downward refraction seems sensible. A thumb rule of one tenth of the maximum range is often suggested as a safe choice in 'folklore'. We have at least found no reason to exceed it.

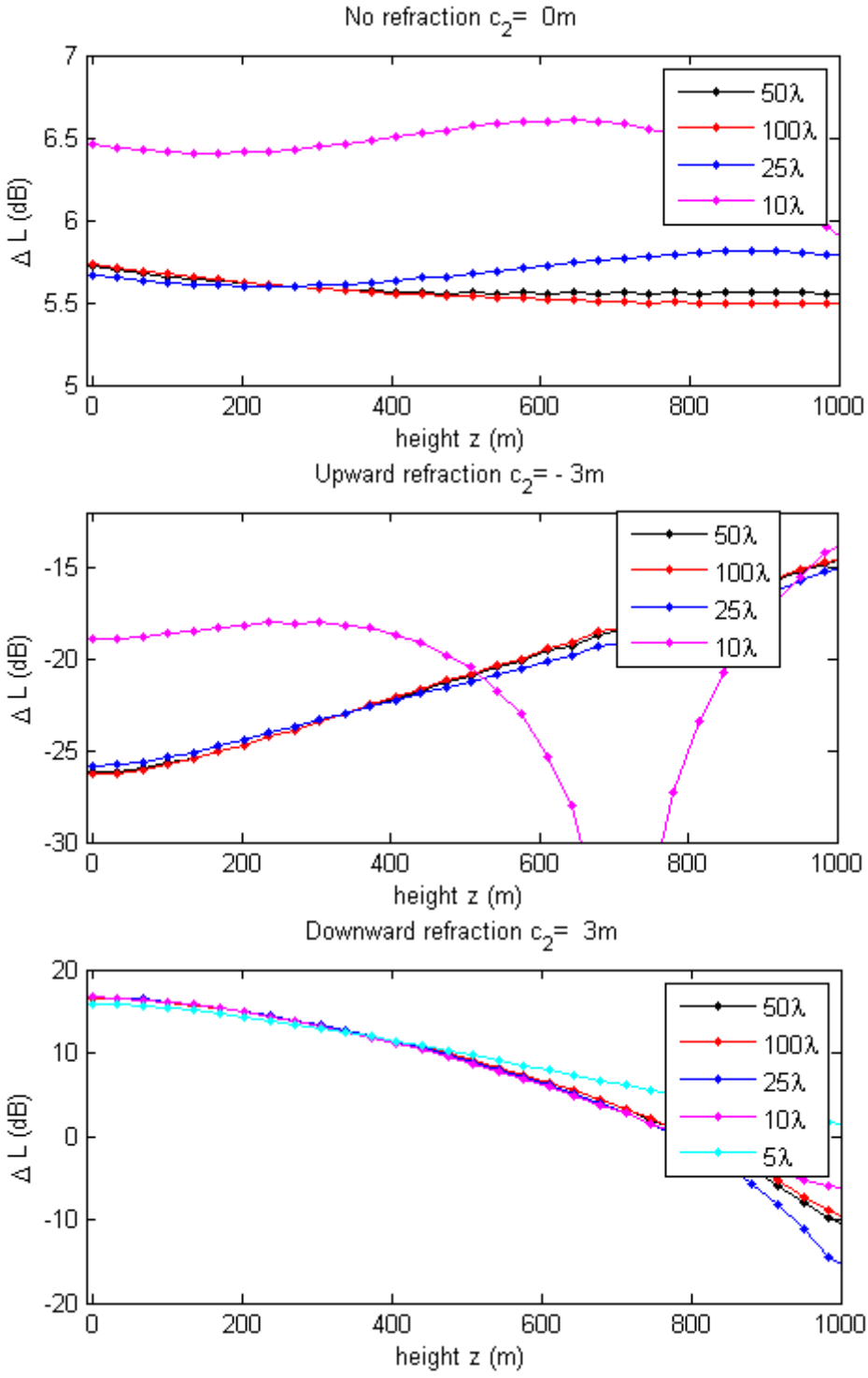

Figure 4.3 Varying thickness of absorption layer. Top: No refraction. Mid: Upward refraction. Bottom: Downward refraction.

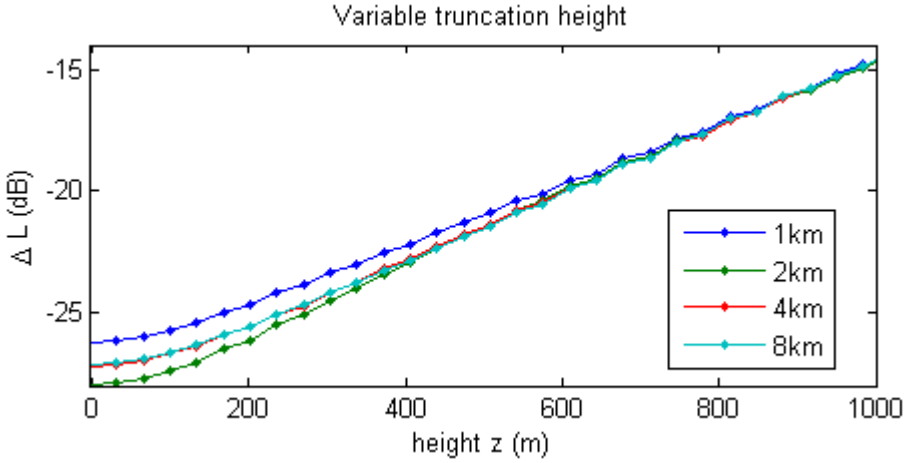

Figure 4.4 Varying truncation heights z_{top}. Same upward refracting profile as in Figure 4.3.

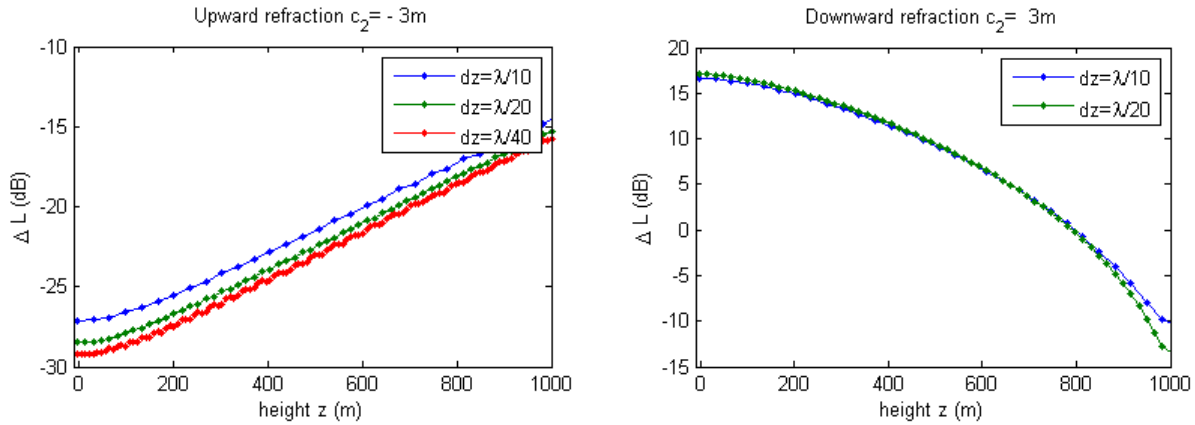

Figure 4.5 Grid resolution for underresolved sound speed gradient. Left: upward refraction, and right: downward refraction.

4.4 Resolution of sound speed gradient

The effective sound speed may change abruptly with height near the ground. Hence, for low frequencies the sound speed gradient will not be represented in much detail with standard grid resolution. We used the same experimental setup as in the previous section to study the need for further refinement. The grid resolution here is 34 m, which drastically reduces the level of detail in the sound speed gradient. Simulation results are shown in Figure 4.5. For upward refraction there is some effect, however it is likely insignificant compared to turbulent scattering. For downward refraction we found little response to refinement beyond standard resolution. It appears that sound speed gradient should not influence resolution.

4.5 Resolution of terrain

We also present a refinement study with terrain features. A sine-shaped hill of width $\lambda/3$ was placed in the propagation path. Standard resolution gave adequate, but limited, accuracy (4.6). For

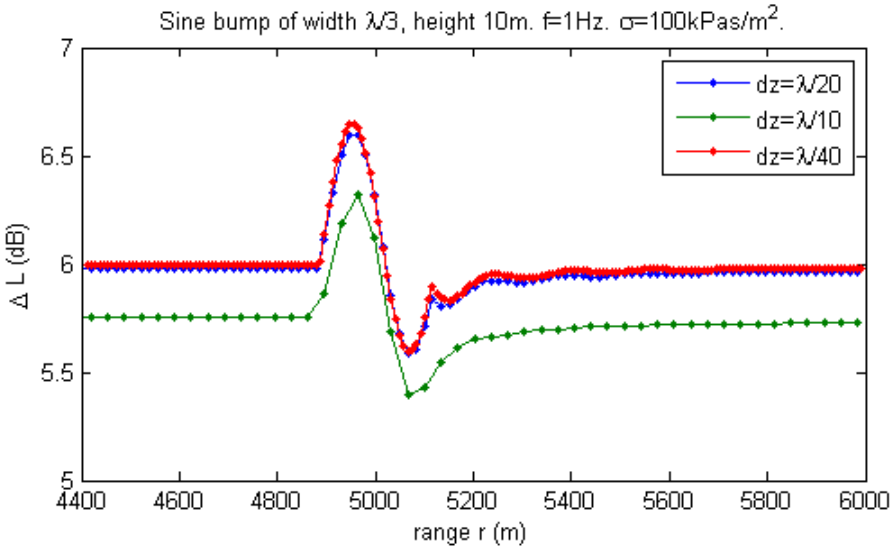

Figure 4.6 Varying grid resoltion with smooth terrain. Fully reflecting ground.

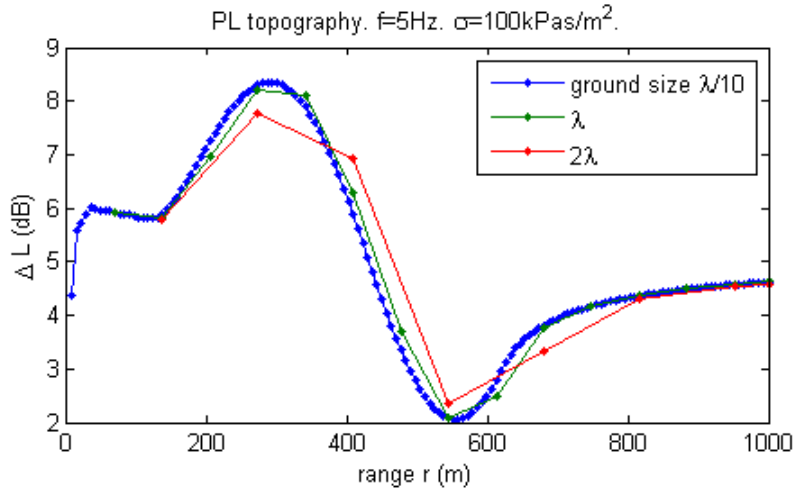

Figure 4.7 Piecewise linear approximation to topography. Different segment length, otherwise same parameters. For reference we plotted the result with segment size equal to grid size $\lambda/10$. The terrain feature was a sine shaped hill of height 40 m and width 500 m.

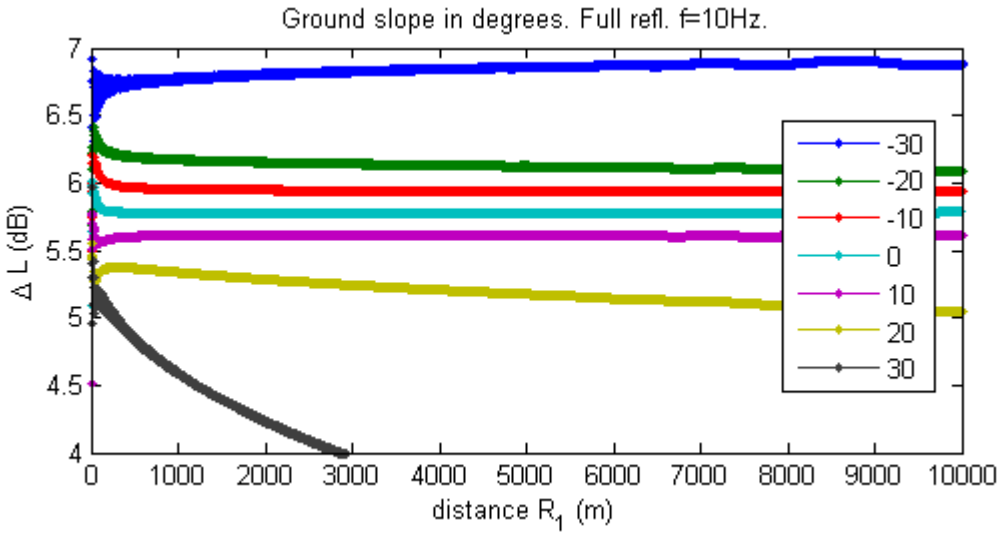

Figure 4.8 Relative sound level for fixed ground slope. Slope angle $\tan^{-1} C$ *is given in degrees. The* x*-axis represents distance along ground.*

efficient computation, it is best to describe the topography with linear segments that are as long a possible, as suggested in [11]. Figure 4.7 shows an experiment with variable segment length. Results are good when the segment length is down to one wavelength. This is enough to speed up calculations. At two wavelengths segment length we also observe decent accuracy but highs and lows are reduced. Probably, the terrain sample points can be chosen smarter to capture peaks and valleys, as opposed to the simple uniform segment size used in this experiment.

4.6 Topographic limitations

The model has inherent limitations when it comes to terrain steepness. Technically, this only affects terrain that has large slope variation, since the r and z-directions are somewhat arbitrarily chosen (although atmospheric stratification gives a guideline). In this test we considered varying spatially constant slope with full ground reflection. Since the directions are arbitrary, results should be identical. Figure 4.8 shows sound levels for varying slope angle. Up to $20°$ results are good, while $30°$ uphill propagation is severely underestimated. Salomons states that GTPE works well if the local slope does not exceed about $30°$. Our experiment suggests $30°$ should at most be attained only over a small region.

4.7 Ground impedance effects

Typical values of resistivity for Norwegian forests are quite low. We expect in the range 10-100 kPa s/m^2. The exact values chosen can play a large role as seen in Figure 4.9. The effect is naturally most pronounced in the case of downward reafraction, while with upward refraction it is more subtle. For this example a logarithmic sound speed profile of strength c_2 =1m/s was used. Since impedance is strongly frequency dependent, ground effect will also be. The purpose

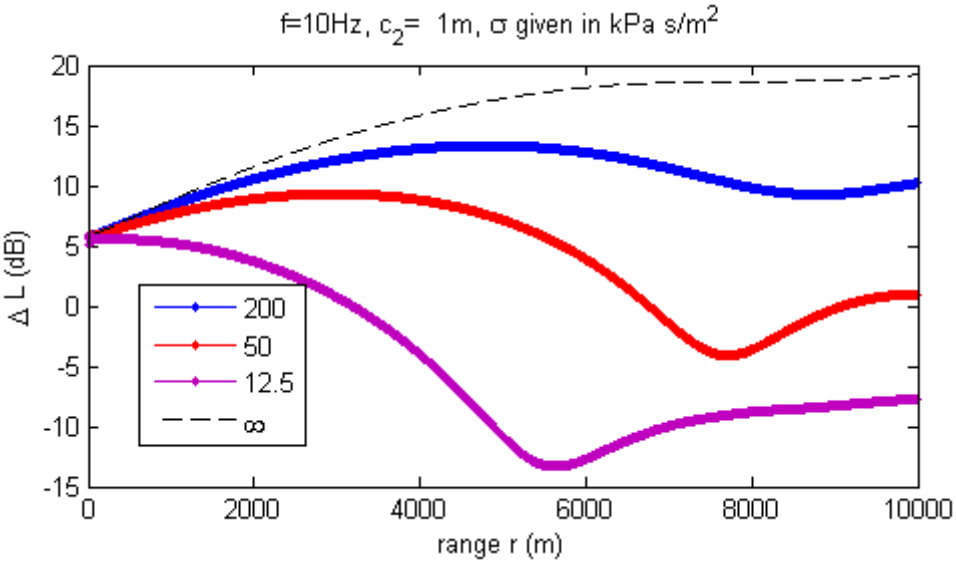

Figure 4.9 Varying the resistivity σ for downward refraction.

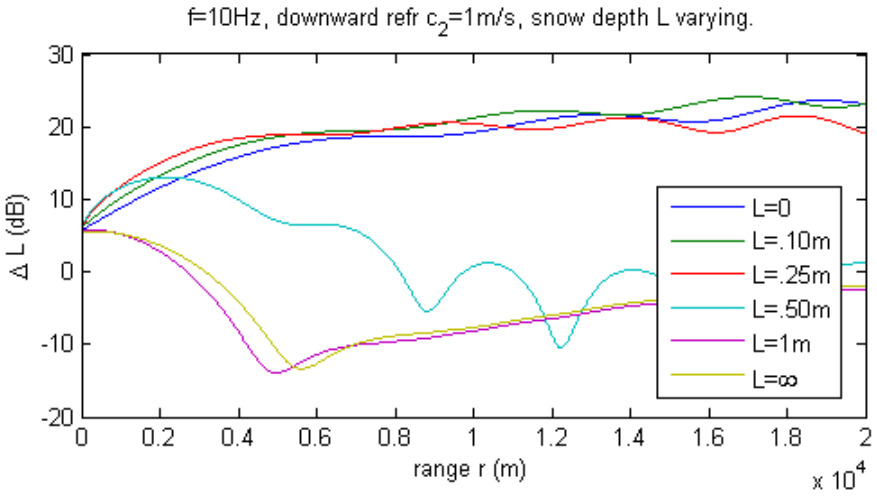

Figure 4.10 Different snow depths over a hard surface. The snow is soft with porosity $\Omega = 0.8$.

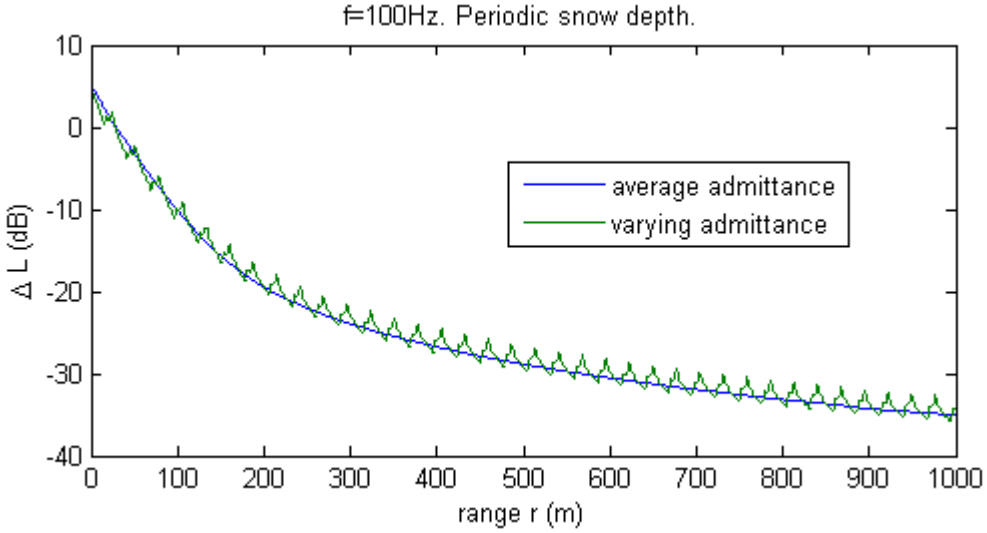

Figure 4.11 Snow depth varies with range as a sinusoid between 0 og 1m, the period is 8λ.

of showing this result is to point out that this is a critical feature of the model, and therefore an important source of parametric (as well as modelling) uncertainty.

The ground effect will vary with season. In particular, frozen ground will reflect more, while snow absorbs noise. Figure 4.10 demonstrates that snow cover can be an important parameter. A layer of soft snow over hard ground is considered. As the snow depth goes from 25 to 100 cm the ground changes type from basically fully reflecting to a soft single layer. Refraction was downward as in Figure 4.9.

Ground characteristics are certainly not spatially constant, and the model can easily accomodate a range-dependent impedance. We therefore present one study where snow depth varies with range, Figure 4.11. The overall effect is absorption, but there are oscillations in the sound levels that follow the snow depth. A natural question to ask is whether there is a single impedance value that characterises the large scale behaviour. We have found that in such cases it is often a good choice to use the average value of admittance $\beta = 1/Z$, and this is illustrated well with this study. In practice, impedance will not be known very precisely. The uncertainty can be modelled stochastically, as suggested in [7] (where range-dependence was ignored). We expect mean admittance to be a key quantity also in the stochastic case. Indeed, a simulation with mean admittance gives the mean complex sound pressure $E(p_c)$ plus an error term proportional to the covariation between β and p_c. In conclusion, sound levels have limited sensitivity to details of ground impedance provided appropriate mean quantities are used. Note that the appropriate range-independent impedance value does not necessarily correspond to any physical range-independent ground configuration.

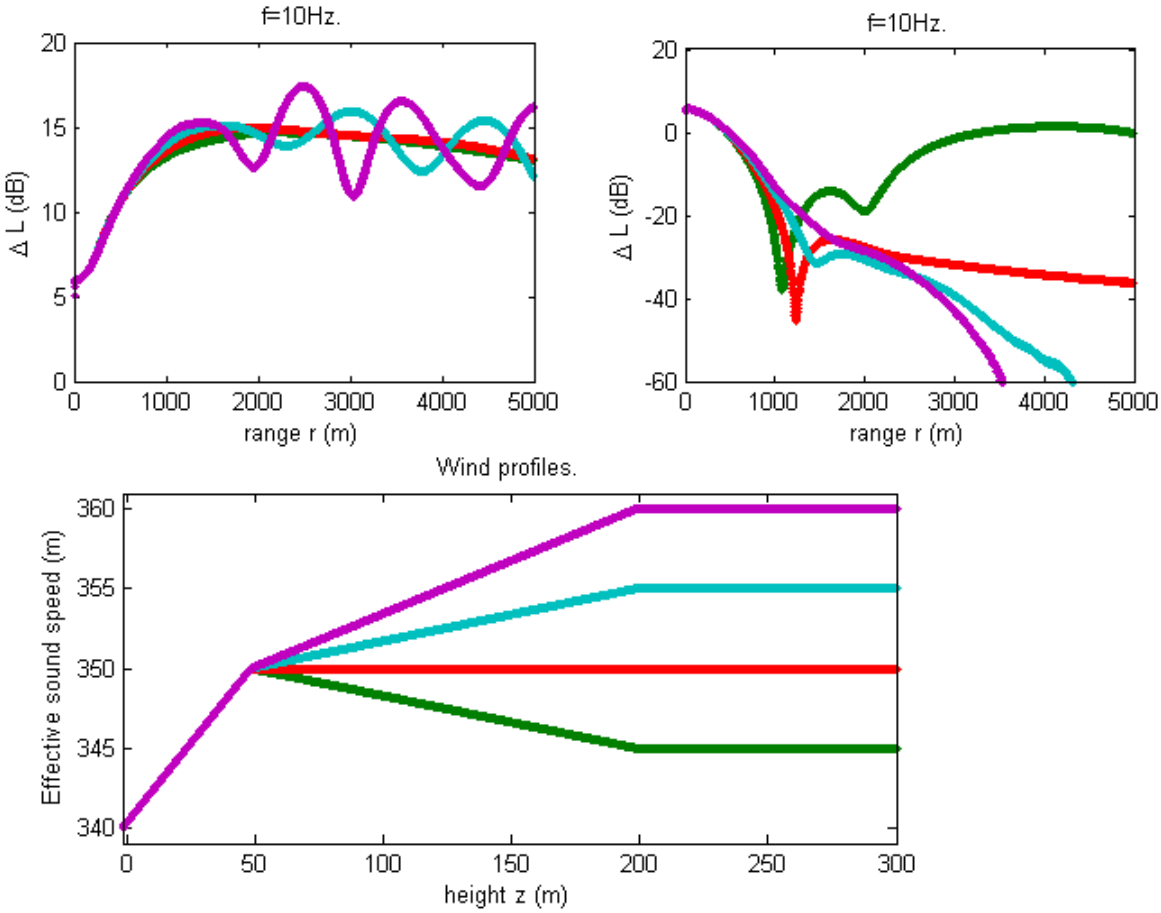

Figure 4.12 Piecewise linear sound speed profile. Top left: upwind, top right: downwind. Soft ground. Bottom: The sound speed profiles (colourmatched) in the upwind case.

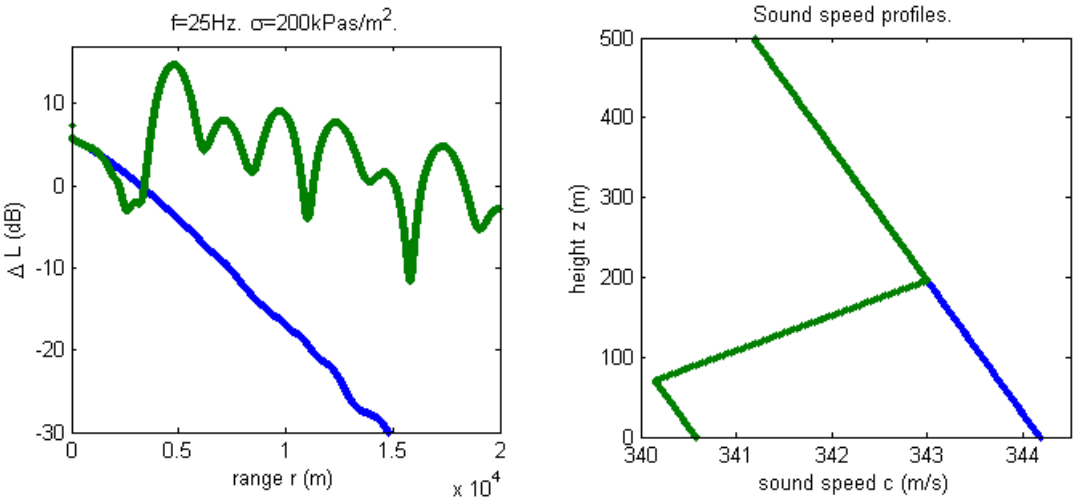

Figure 4.13 An elevated inversion versus an adiabatic lapse rate. The two sound speed profiles are shown on the right.

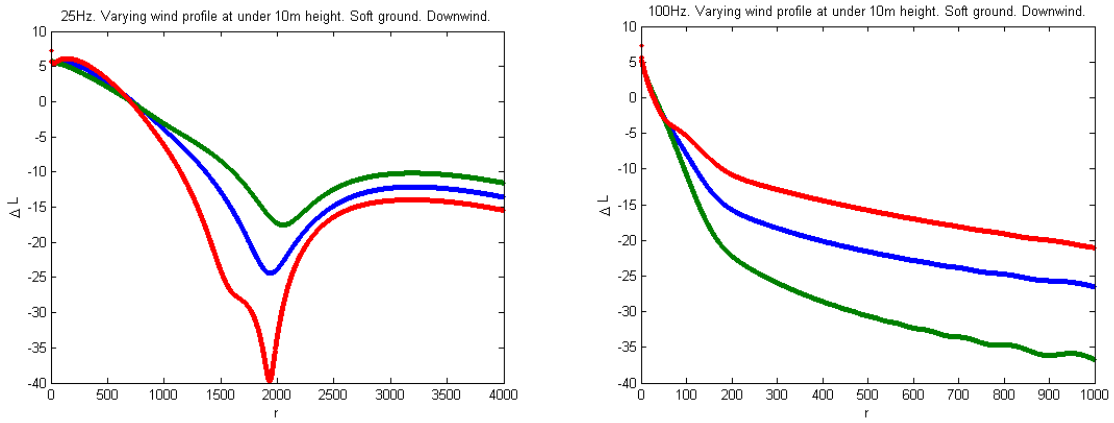

Figure 4.14 Constant sound speed above 10 m (5 m/s in direction of propagation). Varying sound speed profiles underneath. 25 Hz (left) and 100 Hz (right).

4.8 Refraction effects

It is well established that wind and temperature is the major source of variability and uncertainty in sound levels. For long ranges and downward refracting conditions, predictions must take into account conditions several hundred meters up in the atmosphere. We look here at how the sound speed gradient at different heights influence sound levels. For figure 4.12 only the gradient at a medium height between 50 and 200 m height varied for a 10 Hz signal. Below 50 m winds rise linearly to 10 m/s. Both upwind and downwind propagation are considered. As expected, for the first 500 m of propagation, sound levels were the same. In the upwind case we see variation on the order of roughly 5dB due to interference patterns. In the pure downwind case, the exact value of the gradient at the medium height probably matters less, except in an unrealistically narrow interference minimum. The strongest effect is seen when upward refraction near ground is combined with downward refraction higher up. Sound levels are increased with tens of dB compared to the solely upward refracting case. A temperature inversion in remission due to ground heating would look similar, an example of which can be seen in [3] from a tethersonde measurement series. This type of atmospheric condition is very hard to infer from ground measurements. In Figure 4.13 we consider a case roughly corresponding to the measurements from [3]. The elevated inversion case is contrasted with the adiabatic lapse rate observed later in the day. At a distance of a few km, the difference in sound level is dramatic.

We conducted a similar study for the lowest 10 m of the atmosphere. This height was chosen because it is typically the height of meteorological measurements. We find, as could be expected, that for low frequencies, this part of the atmosphere matters little. We show results from f =25 Hz and f =100 Hz. There is a some effect already at 25 Hz. For this experiment we considered downward refraction, with the wind increasing continuously to 5 m/s at 10 m height, then being constant further above.

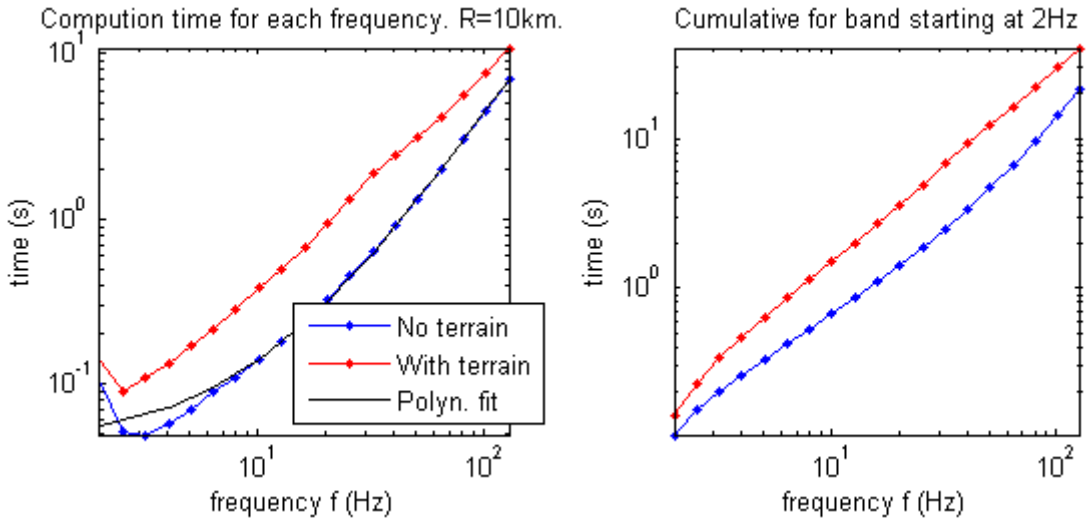

Figure 5.1 Left: Computation time as a function of frequency for a maximum range of 10km. Range sections of size $\max(\lambda, 10\ m)$*. Third octave bands. Right: Corresponding cumulative computation time as* f *increases.*

5 Performance study

In making noise maps, it is necessary to calculate noise for several frequencies, directions, source locations and possibly weather conditions. Computational cost accumulates, and good estimates of computational time is important for choosing strategies of implementation, sampling etc. Some general conclusions can be stated from the form of the numerical schemes. Roughly, the computational time is proportional to the squared frequency f^2. The reason is that the grid size $\Delta z = \Delta r$ is proportiononal to f. Also the domain height is proportional, say one tenth, of the maximum range. For low frequencies, we also need to take the absorption layer into account. More precisely, for a maximum range R, the number of range steps is proportional to $c^{-1}Rf$ and the number of vertical grid cells is proportional to $(50f^{-1} + 0.1Rc^{-1})f$. Hence efficiency should be proportional to $(50 + 0.1Rfc^{-1})Rfc^{-1}$. This is still rough, because the size of the range sections, i. e. the resolution of the terrain, should also be taken into account, and there are costs with setting up the problem etc.

Figure 5.1 shows computation times on a desktop. A range of 2-128 Hz was sampled in third-octaves. First we considered flat ground (blue curve), hence one single range section could be used. A second order polynomial fit is included in the plot, roughly equal to 0.043 s^3 times f^2. For the nonflat case (red curve), each range section was one wavelength long, but we set a minimum range section length to 10 m since available topographic maps are limited. Below 32 Hz (where ($\lambda > 10$ m)), including the terrain increases cost by a factor between 2 and 3. Above, the extra cost gradually decreased as expected. The cumulative cost of calculating for a whole frequency range is most interesting in practice. On the right of Figure 5.1 we see the total cost for different upper cut-off frequencies. Again, we considered third octaves starting with 2 Hz as the lowest frequency. Total time with terrain was 40.7 s and without terrain 21.4 s. If we only consider $f \leq 32$ Hz the

costs are 6.8 s and 2.5 s respectively.

For a practical scenario, we assume that the weather and source position is known, and that noise must be calculated up to a radius of 10 km in all directions. Assuming an angular resolution of five degrees, we have to scale with a factor of 72 to include all directions. As a compromise, we only allow 10 range sections in each direction, which gives no significant cost. We consider third octaves from 2 to 32 Hz as above. Then the total computational cost is about three minutes, which can be acceptable for a local shooting range planner.

A contrastingly demanding scenario is the creation of general purpose noise maps for a shooting range. Let's say the shooting range can be sampled with 100 source locations. We want to fully include topography and average over weather based on 25 weather samples. Frequency is sampled in third-octaves. For 2-128 Hz we end up with 85 days and nights of computing. Although some improvements can probably be made, it will be necessary to use parallel processing to accomplish this. Instead of just averaging over the weather samples etc. it may be more useful to store the sound levels for later use, hence storage requirements are of interest. We assume that for each individual direction and frequency, one sound level value is stored for every $\delta r = \max(\lambda, 10\ \mathrm{m})$. This becomes 10.300 values for the 2-128 Hz band and 4.340 values for the 2-32 Hz band. One byte should be sufficient per data point. The total data amount becomes 75 and 31Mb respectively per weather type, hence a few Gb should suffice.

The absorption layer adds significantly to the cost. Removing the layer reduced computation time by a factor of 57% up to 32 Hz, and 75% up 128 Hz. There are alternative methods to deal with upper truncaation, but each have associated costs. An alternative technique is to use a so called 'Perfectly Matching Layer' in place of the absorption layer. However, an extra layer of thickness 20λ is still required [9]. Also note that in [6] it is pointed out that the PML technique does not perform so well for long-range propagation. As a third alternative, a 'non-local' boundary condition (see [6] for details) was considered, but a more efficient numerical discretisation than we have found in the literature is needed.

6 Summary

We have presented an implementation of a Parabolic Equation Method in Matlab, verified it against known examples, and tested its low frequency performance. There are a number of numerical parameters that determine the accuracy and efficiency of the method, and we have developed recommendations for those. Generally we have found the recommendations in the text book [8] to work well. Although that book focused on higher frequencies (above 100 Hz), we have found the recommendations to largely translate to lower frequencies, at least as long as an accuracy of 1-2 dB is sufficient. Hence, we can use a grid size of a tenth of a wavelength, even though it may seem to result in poorly resolved physical background features. One wavelength appears to be a good thumb rule for the terrain resolution. This parameter should be as large as possible for efficiency, as explained above. Different starting data were considered, and we

recommend the more sophisticated formula given in [8], although it is indicated to be of little importance in that reference.

The domain needs to be artificially truncated above. We use the absorption layer technique to avoid reflections from the artificial boundary. Suitable absorption rates for the lowest frequencies have been determined, and we have found that the recommended absorption layer thickness of 50 wavelengths translates to lower frequencies. This means that the absorption layer may take up a large percentage of computational time. Depending on the frequency band of interest, althernative methods for domain truncation, especially the PML technique, may be worth testing.

Computation times at varying frequencies were measured. They imply that parallel processing is in general necessary to produce noise maps with the PE method. The time needed strongly depends on the frequency band of interest, as the computation time roughly goes as f^2. It is possible to make fairly fast, operational serial versions for a range of about 2-32 Hz, if some compromises are made. Currently, the Milstøy code is not considered very reliable below 25 Hz, hence this is an important conclusion. A different way to employ PE calculations is to produce noise maps for selected parameter samples, which is then used by a table lookup routine.

A stochastic turbulence model for refractive index fluctuations has been implemented. It is a valuable theoretical tool, however it can not be made operationally efficient. With advances in modelling and computational techniques, turbulence models might become operational in the future.

In the PE literature the ground model is nearly always given as a single infinite porous layer under local reaction approximation. We have demonstrated that there is room to soften this restriction by taking a grazing angle limit for the specific impedance Z (by grazing angle we refer to a wave propagating parallel to the ground surface). Specifically, we can model a rigid porous layer over hard ground.

We have included some examples that highlight the importance of physical input parameters, focusing on ground impedance, snow depth and sound speed gradients at different heights. Ground impedance value has a strong effect on sound level, even within the range of values typically considered 'soft', although not as strong an effect as the weather. Tests for range-dependent ground impedance Z, indicated that the average admittance β determines the large scale behaviour in many cases. This might explain why most authors are content with a constant Z-value. For many parameters we have observed a nonlinear relationship with the sound level. Often a saturation effect was seen at extreme ends of the parameter range, especially clearly so in the snow depth study. In the case of upward refraction, the sound levels dropped below realistic values for increasing refraction strength, while for downward refraction the saturation effect was obscured by interference patterns.

References

[1] Keith Attenborough, Ming Li Kai, and Shahram Taherz. *Predicting Outdoor Sound*. Taylor & Francis Ltd, Hoboken, NJ, 2006.

[2] D Heimann and EM Salomons. Testing meteorological classifications for the prediction of long-term average sound levels. *Applied Acoustics*, 65(10):925–950, 2004.

[3] Lars R Hole, Yngvar Gjessing, Tor De Lange, and Jack W Reed. Meteorological measurements and conditions during Norwegian trials. *Noise Control Eng J*, 46(5):199–207, 1998.

[4] M Huseby, R Rahimi, JA Teland, I Dyrdal, H Fykse, B Hugsted, CE Wasberg, E Aker, R Cleave, F Løvholt, H Olsen, SÅ Storeheier, and Taraldsen. G. Final report: Improvement of the computational methods of the Norwegian defence estates agency for computing noise from the Norwegian defence training ranges. *Norwegian Defence Research Establishment report*, 2008.

[5] Morten Huseby. Noise emission data for m109, 155 mm field howitzer, 2007.

[6] Mireille Levy. *Parabolic equation methods for electromagnetic wave propagation*. Number 45. IET, 2000.

[7] Vladimir E Ostashev, D Keith Wilson, and Sergey N Vecherin. Effect of randomly varying impedance on the interference of the direct and ground-reflected waves. *The Journal of the Acoustical Society of America*, 130:1844, 2011.

[8] Erik M Salomons. *Computational Atmospheric Acoustics*. Springer Netherlands, 2001.

[9] Michelle Swearingen. Personal communication.

[10] Michelle E Swearingen and Morten Huseby. Parabolic equation source term issues at low frequencies and long distances. In *INTER-NOISE and NOISE-CON Congress and Conference Proceedings*, volume 2009, pages 427–430. Institute of Noise Control Engineering, 2009.

[11] Michelle E Swearingen, Morten Huseby, and Reza Rahimi. *Comparison of Sound Propagation Codes: Milstoy, BNoise and a PE-method*. Forsvarets Forskningsinstitutt, 2009.

[12] G. Taraldsen. The Delany-Bazley impedance model and Darcy's law. *Acta Acustica united with Acustica*, 91(1):41–50, 2005-01-01T00:00:00.

[13] Gunnar Taraldsen and Hans Jonasson. Aspects of ground effect modeling. *The Journal of the Acoustical Society of America*, 129(1):47–53, 2011.

[14] Jan Arild Teland, Reza Rahimi, and Morten Huseby. Numerical simulation of sound emission from weapons. *Noise Control Engineering Journal*, 55(4):390–396, 2007.

[15] Roger Waxler, Carrick L Talmadge, Shantharam Dravida, and Kenneth E Gilbert. The near-ground structure of the nocturnal sound field. *The Journal of the Acoustical Society of America*, 119:86, 2006.

[16] D Keith Wilson and Chris L Pettit. Effective use of parabolic equation methods for noise prediction. In *INTER-NOISE and NOISE-CON Congress and Conference Proceedings*, volume 2011, pages 1147–1157. Institute of Noise Control Engineering, 2011.